The Astrophysical Journal Letters, 854:L23 (6pp), 2018 February 20 https://doi.org/10.3847/2041-8213/aaacfb

Fermi Transient J1544–0649: A Flaring Radio-weak BL Lac

Gabriele Bruni[1], Francesca Panessa[1], Gabriele Ghisellini[2], Vahram Chavushyan[3], Harold A. Peña-Herazo[3,4,5], Lorena Hernández-García[6], Angela Bazzano[1], Pietro Ubertini[1], and Alex Kraus[7]
[1] INAF—Istituto di Astrofisica e Planetologia Spaziali, via Fosso del Cavaliere 100, I-00133 Roma, Italy; gabriele.bruni@iaps.inaf.it
[2] INAF—Osservatorio Astronomico di Brera, via E. Bianchi 46, I-23807 Merate, Italy
[3] INAOE—Instituto Nacional de Astrofísica Óptica y Electrónica, Apartado Postal 51-216, 72000 Puebla, Mexico
[4] Università degli Studi di Torino—Dipartimento di Fisica, via Pietro Giuria 1, I-10125 Torino, Italy
[5] INFN—Istituto Nazionale di Fisica Nucleare, Sezione di Torino, I-10125 Torino, Italy
[6] IFA—Instituto de Física y Astronomía, Facultad de Ciencias, Universidad de Valparaíso, Gran Bretaña 1111, Playa Ancha, Valparaíso, Chile
[7] MPIfR—Max Planck Institute for Radio Astronomy, auf dem Hügel 69, D-53121 Bonn, Germany
Received 2017 December 11; revised 2018 January 26; accepted 2018 February 3; published 2018 February 16

Abstract

On 2017 May 15, the *FERMI*/LAT gamma-ray telescope observed a transient source not present in any previous high-energy catalog: J1544–0649. It was visible for two consecutive weeks, with a flux peak on May 21. Subsequently observed by a *Swift*/XRT follow-up starting on May 26, the X-ray counterpart position was coincident with the optical transient ASASSN-17gs = AT2017egv, detected on May 25, with a potential host galaxy at $z = 0.171$. We conducted a 4-month follow-up in radio (Effelsberg-100 m) and optical (San Pedro Mártir, 2.1 m) bands, in order to build the overall Spectral Energy Distribution (SED) of this object. The radio data from 5 to 15 GHz confirmed the flat spectrum of the source, favoring a line of sight close to the jet axis, not showing significant variability in the explored post-burst time window. The Rx ratio, a common indicator of radio loudness, gives a value at the border between the radio-loud and radio-quiet active galactic nuclei (AGNs) populations. The Ca_{II} H&K break value (0.29 ± 0.05) is compatible with the range expected for the long-sought intermediate population between BL Lacs and FRI radio galaxies. An overall SED fitting from the radio to gamma-ray band shows properties typical of a low-power BL Lac. As a whole, these results suggest that this transient could be a new example of the recently discovered class of radio-weak BL Lac, showing for the first time a flare in the gamma/X-ray bands.

Key words: BL Lacertae objects: general – gamma-rays: galaxies – radiation mechanisms: non-thermal – radio continuum: galaxies – quasars: general – X-rays: general

1. Introduction

The release of the *Fermi* mission catalog has revealed several unidentified gamma-ray sources, whose association with lower frequency emission is still under study. Among these, radio-weak BL Lac objects (Massaro et al. 2017, and references therein) are challenging our comprehension of the radio-loud phase in active galactic nuclei (AGNs). These extragalactic objects present the same optical properties of BL Lacs—that together with flat spectrum radio quasars define the blazar class—but are radio weak (mostly undetected in major radio surveys). They behave differently from what is expected for these kind of objects, which are normally used as calibrators for radio observatories (e.g., 3C 286, 3C 273, BL Lac, OJ 287). Until now, only a handful of radio-weak BL Lacs have been presented in the literature, and their collocation in the context of the more general unified model of AGN (Urry & Padovani 1995) is still under debate. Indeed, understanding the radio-weak (radio-quiet) AGN population is of crucial importance in order to unveil the conditions that trigger the launching and collimation of relativistic jets, and their relation with other constituents of AGN such as relativistic outflows. Most recent observational results (Boccardi et al. 2016) suggest that the jet base in some sources is wide enough to favor the Blandford & Payne (1982) model, in which the jet can be originated from the accretion disk; BL Lacs are believed to be the low-accreting fraction of the blazar class at the end of an evolutionary track starting from a high-accreting flat spectrum radio quasar (Cavaliere & D'Elia 2002). Thus, radio-weak BL Lacs are the ideal objects to probe the minimum conditions needed to form a jet. Their existence and fraction would also have an impact on the gamma-ray association with radio counterparts, currently based on major radio surveys like FIRST (Becker et al. 1995) and NVSS (Condon et al. 1998), that basically do not include the radio-quiet population lying below the ∼1 mJy flux density threshold.

On 2017 May 15 *Fermi*/LAT detected a transient not associated with any known gamma-ray source. Named *Fermi* J1544–0649, it showed clear detection for two consecutive weeks, with a peak on May 21. It was reported by Ciprini et al. (2017) on June 11, together with a follow-up observation by *Swift*/XRT, measuring an enhancement in X-ray emission at a position corresponding to the optical transient detected on May 25 (ASASSN-17gs = AT2017egv[8]). The host galaxy has been suggested to be 2MASX J15441967–0649156, observed in an optical band as a follow-up of the *Fermi* transient, and for which a redshift of $z = 0.171$ has been estimated (Chornock & Margutti 2017). The source is also present in the NVSS catalog (Condon et al. 1998) with a flux density at 1.4 GHz of 46.6 mJy, and a marginally resolved morphology of about 2′ (see Figure 1). More recently, it has been detected by the TGSS survey at 150 MHz (Intema et al. 2017), performed with the Giant Metrewave Radio Telescope (GMRT), with a flux density of 67 mJy. The flat radio spectrum between these two measurements suggests a blazar-like emission, with the jet oriented toward the observer, but with a power ascribable to

[8] https://wis-tns.weizmann.ac.il/object/2017egv

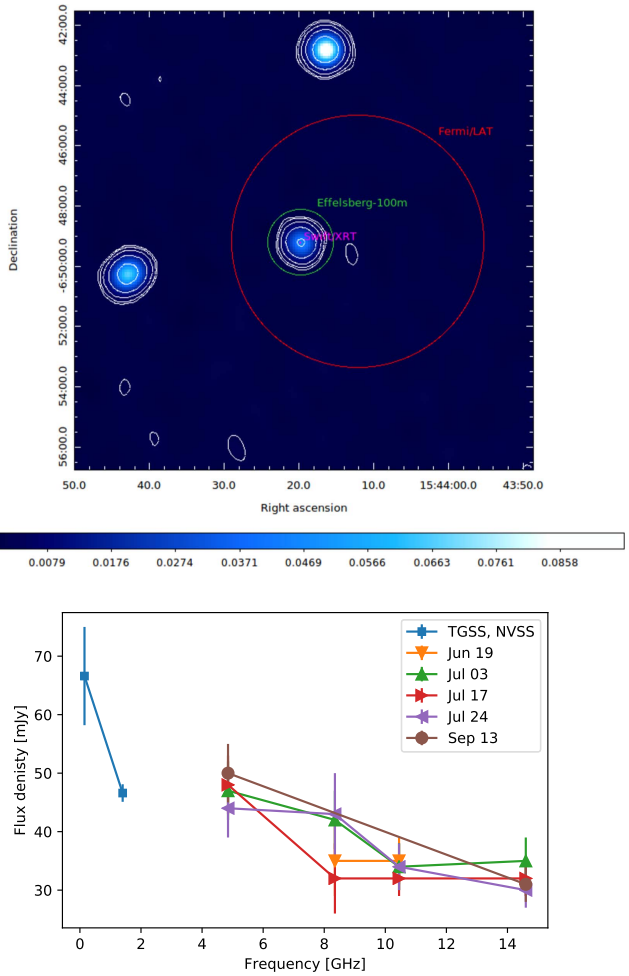

Figure 1. Top panel: NVSS map centered on source J154419–064913. Angular resolution and target positions for Effelsberg-100 m (∼2.5 arcmin at 4.85 GHz), *Swift*/XRT (90% containment radius of 1.4 arcsec), and *Fermi*/LAT (95% containment radius of 0.07 deg) are shown. The flux density scale from NVSS is in Jy/beam and the contours are in the logarithmic scale from 3σ to 1000σ. Bottom panel: Effelsberg-100 m radio SED at different epochs (post-burst), together with flux densities from the literature (TGSS and NVSS, pre-burst).

radio-quiet AGN (see Section 2 for a detailed discussion). Indeed, it has a $L_{1.4\,\mathrm{GHz}} = 3.9 \times 10^{31}$ erg s^{-1} Hz^{-1}, lower than the threshold limit definition ($L_{1.4\,\mathrm{GHz}} = 10^{32.5}$ erg s^{-1} Hz^{-1}; Gregg et al. 1996). This makes this transient a possible candidate for an AGN class still under debate: radio-weak BL Lacs.

2. Observations and Archive Data

2.1. Effelsberg-100 m Single Dish Data

We obtained target of opportunity (ToO) observations with the Effelsberg-100 m single dish radio telescope to monitor the radio spectral energy distribution (SED) of our target in a ∼4-months time window after the Ciprini et al. (2017) discovery. Observations were carried out in cross-scan mode at 4.85, 8.35, 10.45, and 15 GHz in order to cover the entire cm-band. The number of subscans was 16 at 4.85 and 8.35 GHz, and 32 at 10.45 and 15 GHz, reaching a typical rms of ∼2 mJy and ∼1 mJy, respectively. Pointing/focusing on convenient nearby calibrators was performed before each observing slot. The flux density scale was calibrated using

Table 1
Radio Flux Densities Collected with the Effelsberg-100 m Telescope for the Five Post-burst Epochs in 2017

Epoch	Time	4.85	8.35	10.45	14.60	$\alpha_{4.85}^{14.60}$
Jun 19	+35	⋯	35 ± 6	35 ± 4	⋯	⋯
Jul 3	+49	47 ± 5	42 ± 5	34 ± 4	35 ± 4	−0.27 ± 0.25
Jul 17	+63	48 ± 5	32 ± 6	32 ± 3	32 ± 3	−0.37 ± 0.23
Jul 24	+70	44 ± 5	43 ± 7	34 ± 4	30 ± 3	−0.35 ± 0.25
Sep 13	+121	50 ± 5	⋯	⋯	31 ± 3	−0.43 ± 0.23

Note. Days elapsed after the burst are in column 2. The frequencies are in GHz and the flux densities are in mJy (columns 3–6). The last column reports spectral indices between 4.85 and 14.60 GHz.

multiple scans on 3C 286 for each epoch, taking as reference the Baars et al. (1977) scale; given the variable weather conditions, the flux scale uncertainty can be considered ∼10% of the total flux density measurement. Data were reduced in TOOLBOX,[9] extracting the flux densities via the Gaussian fit of the cross-scans. The final error has been calculated via the quadratic sum of the cross-scan rms and the flux scale error.

In total, we collected five epochs at $t = +35$, $+49$, $+63$, $+70$, and $+121$ days after the initial burst detected by *Fermi*. Measurements are reported in Table 1 and plotted in Figure 1; values at the same frequency from different epochs are compatible within errors, not indicating radio variability up to four months after the burst in the gamma-ray band. A correlation between gamma-ray and radio emission in blazars has been found by different authors (Schinzel et al. 2012; Casadio et al. 2015; Chidiac et al. 2016; Karamanavis et al. 2016; Lisakov et al. 2017) with time-lags spanning between days to months for the radio associated emission, and flux density enhancements of a factor of 2 or more. In this case, the low activity of the source could further expand the delay between detection in the different bands, being more than the four months explored here. Another possibility is that the lower energy involved with respect to classic blazars produces a variability magnitude smaller than our error bars from the Effelsberg-100 m measurements (<5 mJy, i.e., <10% of flux density).

The spectral index (α, adopting the convention $S = \nu^{\alpha}$) calculated between 4.85 and 14.60 GHz shows values >-0.5 for all epochs, suggesting an orientation of the jet near the line of sight, typical of blazars. This confirms the estimate at lower frequencies using pre-burst flux densities from the literature, giving an $\alpha = -0.16 \pm 0.21$ between 150 MHz (TGSS, 66.6 ± 8.4 mJy) and 1.4 GHz (NVSS, 46.6 ± 1.5 mJy).

In Figure 1 we show the NVSS map at 1.4 GHz of our target with an angular resolution of 45 × 45 arcsec. Two other intervening sources are visible, but are not related to the emission of the transient. The Effelsberg-100 m angular resolution and pointing position at the lower frequency observed (4.85 GHz) is reported for comparison, together with the *Fermi*/LAT and *Swift*/XRT 95% and 90% containment radius, respectively, from the corresponding ATels. The identification of the *Swift*/XRT transient with the NVSS source is evident, and the lack of other radio counterparts in the *Fermi* and Effelsberg-100 m beams results in a bona-fide association as well. The NVSS map itself shows a marginally resolved structure, with a deconvolved linear size of 15 × 6 arcsec and a position angle of 24°. At the spatial scale of the

[9] https://eff100mwiki.mpifr-bonn.mpg.de/doku.php

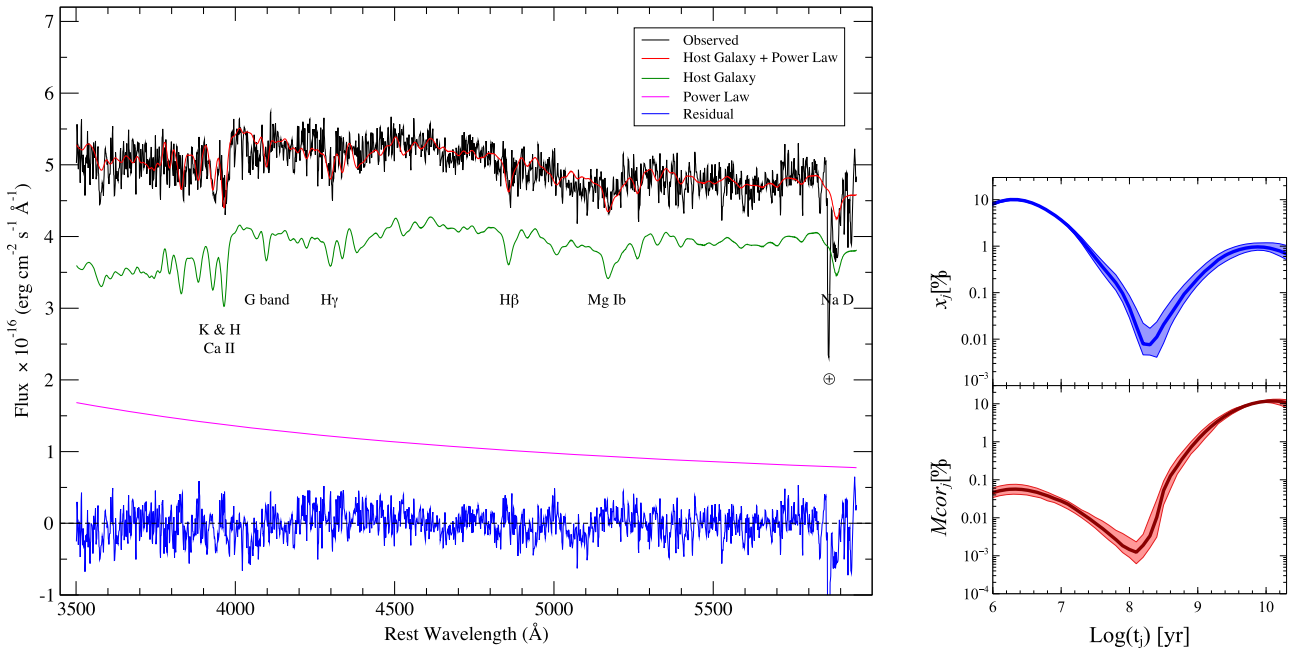

Figure 2. Left panel: spectral synthesis for the object J154419–064913, performed by STARLIGHT using 150 SSP and six power laws to simulate the AGN continuum emission. The observed spectra, host galaxy model, AGN component, and residuals are shown. Right panel: population mixture results obtained for 100 realizations with STARLIGHT. The median curve of the contribution of the light-weighted population vector x_j (blue, top) and the median curve of the contribution of the mass-weighted population vector Mcor_j (red, bottom). Both population vectors are in percentage and logarithmic scale and plotted against each SSP with age t_j. In both of the panels, the shadow regions represent the first and third quartiles.

source (2.912 kpc arcsec^{-1}, for a flat universe with $\Omega_{\rm m} = 0.3$, $\Omega_\Lambda = 0.7$, and $H_0 = 70\,{\rm km\,s^{-1}\,Mpc^{-1}}$; Planck Collaboration et al. 2014), this translates into a projected size of 44 × 17 kpc, comparable with the dimensions of the extended jets from common blazars (e.g., 3C273, BL Lac).

In order to estimate the radio loudness of the source with a further indicator (in addition to the Gregg et al. 1996 mentioned above), we adopted R_X (Terashima & Wilson 2003). For this calculation we used the post-burst data at 5 GHz from our Effelsberg-100 m campaign, and the flux from *Swift*/XRT published in Sokolovsky et al. (2017). We obtained a value of Log(Rx) = −4.3, near to the limit of −4.5 considered by Terashima & Wilson (2003), to divide the radio-loud and radio-quiet populations. This value is also in the range obtained for the Seyfert galaxies by the same authors.

2.2. Optical Observations

Optical spectra were obtained with the 2.1 m telescope of the Observatorio Astronómico Nacional at San Pedro Mártir (OAN-SMP), Baja California, México, on 2017 August 23 (start at 03:30 UT). Clear sky conditions were present, with a seeing of 2.1 arcsec. The Boller & Chivens spectrograph was tuned to the 3800–8000 Å range (grating 300 l/mm) with a spectral dispersion of 4.5 Å/pix, corresponding to 10 Å FWHM derived from the FWHM of different emission lines of the arc-lamp spectrum. A 2.5 arcsec slit was used. To calibrate the spectral measurements, the spectrophotometric standard star Feige 110 was observed at night.

The data reduction was carried out with the IRAF[10] software following standard procedures. The spectra were bias-subtracted and corrected with dome flat-field frames. Cosmic rays were removed interactively from all of the images. Arc-lamp (CuHeNeAr) exposures were used for the wavelength calibration. A spline function was fitted to determine the dispersion function (wavelength-to-pixel correspondence). Sky emission lines located at known wavelengths were removed during the calibration in the wavelength. The obtained spectrum is shown in Figure 2.

2.2.1. Black Hole Mass Estimate

To evaluate the central black hole mass, we used the stellar population synthesis code STARLIGHT. A detailed description of the STARLIGHT code can be found in the publications of the Semi Empirical Analysis of Galaxies (SEAGal) collaboration (Cid Fernandes et al. 2005, 2007). Before running STARLIGHT we carried out the pre-processing steps required for the code implementation. First, the spectra were corrected for Galactic extinction assuming an $E(B-V)$ value of 0.156, as computed by Schlegel et al. (1998). Extinction in the galaxy is taken into account in the synthesis, assuming that it arises from a foreground screen with the extinction law of Cardelli et al. (1989). We derived information about the stellar populations of the host galaxy in the STARLIGHT analysis. To simplify the analysis we decided to define the intervals of young ($t_j < 10^8$ year), intermediate ($10^8 \leqslant t_j \leqslant 10^9$ year), and old ($t_j > 10^9$ year) stellar populations as stated in Cid Fernandes et al. (2005). The best fit is a combination of 150 single stellar populations (SSP) from the evolutionary synthesis models of Bruzual & Charlot (2003) and six power laws to represent the AGN continuum emission (see Figure 2; e.g., León-Tavares et al. 2011). Since BL Lacs are characterized by strong non-thermal emission at all frequencies from compact components with power-law continua, spectral indices of −0.5, −1.0, −1.5, −2.0, −2.5, and −3.0 were used to represent non-thermal jet emission typically observed in these AGN. As

[10] IRAF is distributed by the National Optical Astronomy Observatories operated by the Association of Universities for Research in Astronomy, Inc. under cooperative agreement with the National Science Foundation.

we can observe in Figure 2, the light-weighted population vector is dominated (∼90%) by a young stellar population although the contribution of this population to the mass-weighted population vector is less than 1%, which can be explained by a recent star formation event. Moreover, we did not observe a significant contribution of the intermediate stellar population. In contrast, the old stellar population represents nearly 97% of the mass-weighted population vector Mcor_j and 9% of the light-weighted population vector, in agreement with the elliptical nature of the host galaxy of BL Lacertae objects.

We estimate the $M_{\rm BH}$ from the velocity dispersion derived with STARLIGHT. Assuming an average instrumental resolution, from the FWHM of the sky lines, of 18.5 Å in the range between 4000 and 7000 Å, this yields a corrected stellar velocity dispersion of 252 ± 43 [km s^{-1}]. Using the M–σ relation in Tremaine et al. (2002) we estimate a black hole mass of $M_{\rm BH} = 3.4 \pm 1.4 \times 10^8\,[M_\odot]$.

2.2.2. Ca_{II} H&K Break

To assess the spectral classification of our target, we measured the Ca_{II} H&K break from the optical spectrum (Landt et al. 2002). The value of the Ca_{II} break of $C = 0.29 \pm 0.05$ ensures that the galaxy is dominated by the thermal spectrum of the host rather than the non-thermal spectrum of an active nucleus or a relativistic jet. Landt et al. (2002) find that Ca_{II} H&K break values $0.25 < C < 0.4$ could represent the long-sought population intermediate between the classical BL Lacs and the FRI radio galaxies. Still, the same authors suggest that a value of 0.35 can be assumed for separate BL Lacs and radio galaxies, which makes our object a member of the first class.

2.3. Multi-wavelength SED Fitting

In order to compile a pre-burst multi-wavelength SED, we collected the available archive data with the ASI Science Data Center (ASDC) online tool.[11] In addition to that, we considered the upper limit from *INTEGRAL/ISGRI* measurements of the field corresponding to our target position, resulting from the first 1000 orbit observations (Bird et al. 2016) in the 20–40 KeV band ($<3.8 \times 10^{-12}$ [erg cm^{-2} s^{-1}]). As post-burst data, we used the second Effelsberg-100 m epoch (for which 4 frequencies were available), the *Swift*/UVOT data corresponding to the first *Swift*/XRT follow-up, and obviously the *Swift*/XRT spectrum itself, together with the *Fermi* one.

The overall SED of 1544–9649 shows the typical two-hump shape of blazars, commonly interpreted by a synchrotron and inverse Compton emission from a relativistic jet. Figure 3 shows the overall SED, and compares it with the one of Mkn 501, a typical low-power, high-energy peaked BL Lac object. In both objects the host galaxy emission dominates the optical luminosity, both have a rising (in νF_ν) spectrum in X-rays and in gamma-rays, and both show a large amplitude variability. These similarities suggest that 1544–0649 is a blue BL Lac object, but is more luminous (in its high state) than Mkn 501.

To reproduce the overall SED, we use the model fully described in Ghisellini & Tavecchio (2009). This model assumes that most radiation is produced by relativistic electrons located at a distance $R_{\rm diss}$ from the black hole. The emitting plasma is moving at a relativistic velocity, βc, corresponding to the bulk Lorentz factor Γ. The viewing angle, $\theta_{\rm v}$, is small, so that the relativistic Doppler factor is $\delta \equiv 1/[\Gamma(1 - \beta\cos\theta_{\rm v}] > 1$.

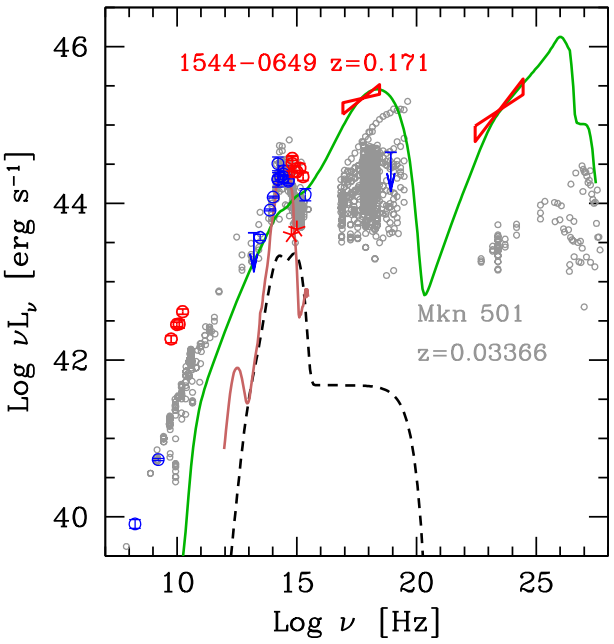

Figure 3. SED of 1544–0649 (blue and red symbols) compared with archival of data of Mkn 501 (gray circles) taken from ASDC. The red points correspond to the flare and post-flare emission and the blue points correspond to the pre-flare epoch. The solid green lines refer to the theoretical model, while the red solid line corresponds to a template for a typical host galaxy of BL Lac objects (Silva et al. 1998). The dashed black line is the spectrum of an accretion disk, together with the IR torus radiation and the X-ray produced in the corona. The two humps in gamma-rays correspond to the peak of the first and second order Compton scattering.

The emitting particle energy distribution is derived solving a continuity equation accounting for radiative cooling and electron–positron pair production and the contribution of these pairs to the observed flux.

The emission processes are synchrotron, synchrotron self-Compton (SSC), and inverse Compton scattering of photons produced externally to the jet (EC), by the disk, by the broad line region, and by the molecular torus.

To account for the fast variability observed in BL Lacs, the source is generally assumed as compact, located at a $R_{\rm diss} = 900$ Schwarzschild radii, and having a size 10 times less (we are assuming that the jet is conical with a semi-aperture angle $\psi = 5°$). The compactness of the source implies that the synchrotron spectrum is self-absorbed below ∼100 GHz, and therefore cannot account for the radio flux at smaller frequencies. This has to be produced by other, more extended portions of the jet.

2.3.1. SED Properties

Figure 3 shows the overall SED of 1544–0649 together with our model, and Table 2 lists the parameters used. The SED of the host galaxy (red solid line) is obtained using the template of a giant elliptical galaxy from Silva et al. (1998), while for the optical emission of the jet we have assumed the decomposition shown in Figure 3.

[11] http://tools.asdc.asi.it/

Table 2
Adopted Parameters for the Jet Models

z (1)	M (2)	L_d (3)	L_d/L_{Edd} (4)	R_{diss} (5)	R_{BLR} (6)	R_{torus} (7)	$P'_{e,jet,45}$ (8)	B (9)	Γ (10)	θ_V (11)	δ (12)
0.171	3.4e8	8.9e-4	5e-4	16.3	81.6	372	9e-5	0.32	16.3	2	24.6

Note. Column (1): redshift; column (2): black hole mass in solar masses; column (3): disk luminosity in units of 10^{45} erg s^{-1}; column (4): disk luminosity in units of the eddington luminosity; column (5): distance of the dissipation region from the black hole, in units of 10^{15} cm; column (6): size of the BLR, in units of 10^{15} cm; column (7): size of the torus, in units of 10^{15} cm; column (8): power injected in the jet in relativistic electrons, calculated in the comoving frame, in units of 10^{45} erg s^{-1}; column (9): magnetic field in G; column (10): bulk lorentz factor; column (11): viewing angle in degrees; column (12): relativistic doppler factor.

The model can capture some of the main features of the SED, but it fails to reproduce the shape of the γ-ray emission and the radio flux. As mentioned, the latter can be produced by other, less compact regions of the jet. The disagreement with the gamma-ray slope can instead be due to some reprocessing of the emission. At a $z = 0.171$, in fact, the IR background can absorb part of the high-energy radiation, producing electron–positron pairs that, in turn, interact with the cosmic microwave background through the inverse Compton process, producing photons that are still gamma-rays, but of smaller energies. This process could then soften the observed gamma-ray slope.

The parameters used for the model (see Table 2) are rather typical for low-power BL Lac objects, whose SED peaks at X-ray energies (synchrotron) and in the TeV band (inverse Compton).

3. Conclusions

Blazar physics has received a tremendous boost from modern-era space missions like *Swift*, *INTEGRAL*, and *Fermi*. Many extragalactic sources detected in recent gamma-ray catalogs by *Fermi* have been matched with known radio-loud blazars, and daily/weekly light curves have allowed detailed correlation for the variability of such sources for the first time, putting a milestone in the understanding of jet launching/collimation mechanisms. A new intriguing class of objects is arising from radio/gamma correlation: radio-weak BL Lacs.

In this work we present the results of a radio/optical follow-up of a gamma-ray flare for one of these objects. We can summarize the results as follows:

(1) The detected flat radio SED confirmed a BL Lac nature with an orientation close to the line of sight, and did not show variability on a 4-month time window. A low-radio power, as measured from the Rx factor, suggests that this object is at the boundaries between the radio-loud and radio-quiet populations.

(2) The disk luminosity in Eddington units (see Table 2) is lower than the known typical values for RL and RQ AGN, as well as for blazars (0.02–0.2, Ghisellini & Tavecchio 2015). In the light of the evolutionary track between flat spectrum radio quasars and BL Lacs proposed by Cavaliere & D'Elia (2002), this could suggest that radio-weak BL Lacs can experience flaring episodes in X/gamma-ray bands, despite the low accretion foreseen for objects at the end of the blazar sequence.

(3) The intermediate properties between the FRI and BL Lac classes, indicated by the Ca_{II} H&K break value, confirm the mixed state of this source.

(4) Finally, the overall SED fitting, from the radio to the gamma-ray band, is typical of a low-power blue BL Lac.

From these results, we can conclude that the nature of this class of objects could probe the minimum conditions for the BL Lac class, both in terms of multi-wavelength variability and jet radio power. The lack of correlation in the explored time window between the gamma-ray band flux enhancement and radio activity in the GHz domain could be symptomatic of a less efficient jet collimation, favoring a fast adiabatic expansion of the particle blobs responsible for the radio emission. This could smooth the additional contribution from newly injected particles. Another possibility is that the distance between the location of the gamma-ray emitting region (i.e., the jet acceleration and collimation zone) and the mm-wave core (Marscher et al. 2008) is larger than that in more powerful BL Lacs. Conversely, the blob speed could be lower, causing a further delay in the correlated radio flux enhancement.

The availability of future instruments like SKA in the radio band and CTA in the gamma-ray band will make it possible to discover and study in more detail populations of intermediate objects like this one, probing the minimum conditions for jet formation and collimation in the AGN population.

We thank F. Tavecchio for useful discussions. This publication has received funding from the European Union's Horizon 2020 research and innovation programme under grant agreement No. 730562 [RadioNet]. We acknowledge support from a grant PRIN-INAF SKA-CTA 2016. G.B. acknowledges financial support under the *INTEGRAL* ASI-INAF agreement 2013-025. R01. V.C. and H.A.P.H. acknowledge support from CONACyT research grant 280789. L.H.G. acknowledges support from FONDECYT through grant 3170527. This work is based on observations with the 100 m telescope of the MPIfR (Max-Planck-Institut für Radioastronomie) at Effelsberg and observations carried out at the Observatorio Astronómico Nacional on the Sierra San Pedro Mártir (OAN-SPM), Baja California, México. Part of this work is based on archival data, software, or online services provided by the ASI SCIENCE DATA CENTER (ASDC).

ORCID iDs

Gabriele Bruni https://orcid.org/0000-0002-5182-6289
Francesca Panessa https://orcid.org/0000-0003-0543-3617
Angela Bazzano https://orcid.org/0000-0002-2017-4396

References

Baars, J. W. M., Genzel, R., Pauliny-Toth, I. I. K., et al. 1977, A&A, 61, 99
Becker, R. H., White, R. L., & Helfand, D. J. 1995, ApJ, 450, 559
Bird, A. J., Bazzano, A., Malizia, A., Fiocchi, M., et al. 2016, ApJS, 223, 15
Blandford, R. D., & Payne, D. G. 1982, MNRAS, 199, 883
Boccardi, B., Krichbaum, T. P., Bach, U., et al. 2016, A&A, 588, L9
Bruzual, G., & Charlot, M. J. 2003, MNRAS, 344, 1000
Cardelli, J. A., Clayton, G. C., & Mathis, J. S. 1989, ApJ, 345, 245
Casadio, C., Gómez, J. L., Jorstad, S. G., et al. 2015, ApJ, 813, 51
Cavaliere, A., & D'Elia, V. 2002, ApJ, 571, 226
Chidiac, C., Rani, B., Krichbaum, T. P., et al. 2016, A&A, 590, A61
Chornock, R., & Margutti, R. 2017, ATel, 10491
Cid Fernandes, R., Asari, N. V., Sodré, L., et al. 2007, MNRAS, 375, L16

Cid Fernandes, R., Mateus, A., Sodré, L., et al. 2005, MNRAS, 358, 363
Ciprini, S., Cheung, C. C., Kocevski, D., et al. 2017, ATel, 10482
Condon, J. J., Cotton, W. D., Greisen, E. W., et al. 1998, AJ, 115, 1693
Ghisellini, G., & Tavecchio, F. 2009, MNRAS, 397, 985
Ghisellini, G., & Tavecchio, F. 2015, MNRAS, 448, 1060
Gregg, M. D., Becker, R. H., White, R. L., et al. 1996, AJ, 112, 407
Intema, H. T., Jagannathan, P., Mooley, K. P., et al. 2017, A&A, 598, A78
Karamanavis, V., Fuhrmann, L., Krichbaum, T. P., et al. 2016, A&A, 586, A60
Landt, H., Padovani, P., & Giommi, P. 2002, MNRAS, 336, 945
León-Tavares, J., Valtaoja, E., Chavushyan, V. H., et al. 2011, MNRAS, 411, 1127
Lisakov, M. M., Kovalev, Y. Y., Savolainen, T., Hovatta, T., & Kutkin, A. M. 2017, MNRAS, 468, 4478
Marscher, A. P., Jorstad, S. G., D'Arcangelo, F. D., et al. 2008, Natur, 452, 7190
Massaro, F., Marchesini, E. J., D'Abrusco, R., et al. 2017, ApJ, 834, 113
Planck Collaboration, Ade, P. A. R., Aghanim, N., et al. 2014, A&A, 571, A16
Schinzel, F. K., Lobanov, A. P., Taylor, G. B., et al. 2012, A&A, 537, A70
Schlegel, D. J., Finkbeiner, D. P., & Davis, M. , 1998, ApJ, 500, 525
Shen, Y., Richards, G. T., Strauss, M. A., et al. 2011, ApJS, 194, 45
Silva, L., Granato, G. L., Bressan, A., et al. 1998, ApJ, 509, 103
Sokolovsky, K., Cusano, F., Dominik, M., et al. 2017, ATel, 10642
Terashima, Y., & Wilson, A. S. 2003, ApJ, 583, 145
Tremaine, S., Gebhardt, K., Bender, R., et al. 2002, ApJ, 574, 740
Urry, C. M., & Padovani, P. 1995, PASP, 107, 803